

LIPS: A Light Intensity Based Positioning System For Indoor Environments

Bo Xie, Guang Tan, *Member, IEEE*, Yunhuai Liu, *Member, IEEE*, Mingming Lu, *Member, IEEE*, Kongyang Chen, and Tian He, *Senior Member, IEEE*



Abstract—This paper presents *LIPS*, a Light Intensity based Positioning System for indoor environments. The system uses off-the-shelf LED lamps as signal sources, and uses light sensors as signal receivers. The design is inspired by the observation that a light sensor has *deterministic sensitivity* to both distance and incident angle of light signal, an under-utilized feature of photodiodes now widely found on mobile devices. We develop a stable and accurate light intensity model to capture the phenomenon, based on which a new positioning principle, *Multi-Face Light Positioning* (MFLP), is established that uses three collocated sensors to uniquely determine the receiver's position, assuming merely a *single* source of light. We have implemented a prototype on both dedicated embedded systems and smartphones. Experimental results show average positioning accuracy within 0.4 meters across different environments, with high stability against interferences from obstacles, ambient lights, temperature variation, etc.

1 INTRODUCTION

The prospect of indoor location based services (LBS) and the unfortunate unavailability of GPS signals indoors have fueled much interest in indoor positioning techniques recently. Among the numerous approaches to achieving such a service, the radio-frequency (RF) based positioning technique has attracted perhaps the most attention, due to the wide deployment of WiFi access points. A major challenge faced by this approach is that RF is subject to serious multipath effect and is vulnerable to environmental interferences. This makes it difficult to establish an accurate propagation model that allows accurate distance estimation. Recent work has focused on the RF fingerprint approach, which obviates the need of a propagation model, but then requires manual efforts to establish a fingerprint database in support of mapping from signal strengths to positions. The fingerprint collection process is often laborious, leading to various research efforts to reduce the cost



Fig. 1: LED lamps and light sensors. (a) LED lighting in an airport terminal. (b) LED lighting in a large warehouse. (c) An infrared LED lamp, 8 watts. (d) A high-power visible light LED lamp, 100 watts. (e) A smartphone with a light sensor (enclosed by red square).

(e.g., [12], [45]). Despite significant advances made in this direction, a fully automatic solution for general indoor environments has remained open.

In this paper we explore an alternative approach, using visible or infrared (IR) light signal rather than RF, to achieving indoor positioning. The main advantage of light signal over RF is that the propagation of light is more predictable than that of RF. This is because on ordinary objects such as walls and furniture, the light signal experiences only insignificant reflection, thus the signal at a receiver is subject to negligible multipath effect. This largely eliminates the uncertainty in characterization of received signal strength (RSS), laying a sound basis for further modeling and derivation of position.

Our system, called *LIPS*, uses commodity LED lamps (see Figure 1) as signal sources, and uses light sensors available on mainstream mobile devices as signal receivers. A low-end microcontroller is used to make the LED lamp switch on and off at specified frequencies, so that the light signals from sources of interest can be separated from ambient ones in the frequency domain. The recovered light signal strength on the light sensor reliably reflects the sensor's distance and orientation with respect to the lamp. This allows one to

- Bo Xie, Guang Tan and Kongyang Chen are with SIAT, Chinese Academy of Sciences. E-mail: {bo.xie, guang.tan, ky.chen}@siat.ac.cn.
- Yunhuai Liu is with Third Research Institute of the Ministry of Public Security, China. E-mail: yunhuai.liu@gmail.com.
- Mingming Lu is with Central South University, China. E-mail: ming.lu@gmail.com.
- Tian He is with University of Minnesota, U.S. E-mail: tianhe@cs.umn.edu.

establish an accurate RSS model which paves the way to *fingerprint-free* positioning. From a practical point of view, the LIPS design could re-use the existing lighting infrastructure for indoor positioning in many public environments, such as airport terminals (Figure 1(a)), warehouses (Figure 1(b)), shopping malls, and hospitals, where lamps are extensively deployed. These lamps can conveniently serve as positioning references, provided they are distinguishable in the frequency domain with different flashing rates and have known positions.

Compared to the RF-based approach, LIPS essentially trades off obstacle penetration ability for improved predictability of signal propagation. The design is centered around two questions: (1) *how accurate and stable is a light sensor in producing position-related information*, and (2) *how to exploit that information for positioning while minimizing the line-of-sight limitation of light signal*? To explore these issues we make three contributions.

First, we conduct comprehensive experiments showing that a light sensor can be used to infer not only distance, but also *angular* information from light signal, with a highlight on its *sensitivity* and *stability*. The angular information turns out to be very useful for obtaining the position of a light sensor.

Second, we develop novel methods for positioning. In particular, we propose a *Multi-Face Light Positioning* (MFLP) method, which uses three collocated sensors to uniquely determine the receiver's position, assuming merely a *single* source of light. This single-source positioning method alleviates the concern of possible high deployment density of light sources, especially in a complex environment, where the light signal's line-of-sight restriction makes it expensive to circumvent obstacles. We show that in such an environment, MFLP requires far less than 1/3 (the theoretical ratio) of the lights as required by trilateration for the same degree of coverage, thus slashes the deployment cost to more accessible levels. In a real environment, different lamps flash at different rates, so they can be distinguished in the frequency domain.

Last, we present two designs for indoor positioning, one for a dedicated receiver and the other for smartphones. We evaluate the systems in various realistic environments and show that LIPS can produce positioning accuracy below 0.4 meters on the average, and that is stable across significant environmental variations.

2 LIGHT SENSOR CHARACTERISTICS

In order to examine the characteristics of a light sensor under different light frequencies and power supplies, we considered two typical types of LED lamps,

- An IR LED lamp, with a 8 watts power rating and a 12 volts DC power supply (see Figure 1(c)), as well as an illuminating angle of 120 degrees. It has a sensing range of 7.5 meters for the sensor, covering an open area of 130 m² on the ground when hung on a 3-meter high ceiling.

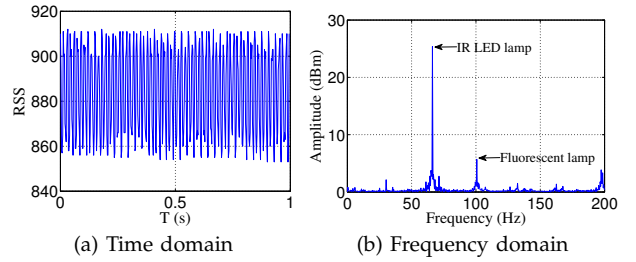


Fig. 2: RSS in the time domain and frequency domain (excluding the DC component). The LED lamp flashes at a frequency of 65 Hz, and the nearby fluorescent lamps flash at a frequency of 100 Hz.

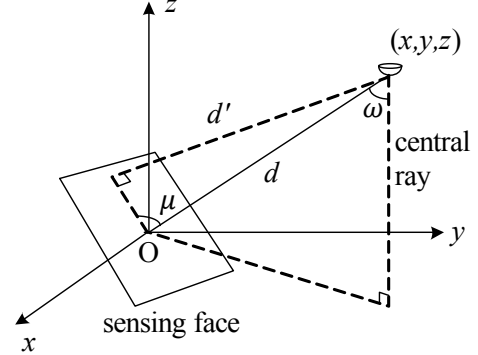


Fig. 3: RSS model of the light sensor. The light sensor's surface (sensing face) is centered at $(0, 0, 0)$, while the lamp is located at (x, y, z) . The RSS of the sensor, s , is a function of distance d , incident angle μ , and emitting angle ω .

- A visible light LED lamp, with a 100 watts power rating (see Figure 1(d)), and a sensing range of 30 meters, covering 2000+ m² in open space when hung at a proper height.

Each lamp has a small illuminating chip of size around 1.5cm \times 1.5cm, thus can be viewed as a point source of light from a distance of a few meters. For space reasons we focus on the IR lamp and only briefly report on the visible light one. In practice, IR lamps can be deployed in environments where there already exist lighting devices and extra visible lights are undesirable.

The light sensor used is an Intersil ISL29023¹, which is used by Samsung Omnia II GT-I8000 smartphone. We used a stand-alone sensor connected to a microcontroller for the experiment.

In reality, what the sensor receives is a mixture of the light signals from the sources of interest and the background, including daylight and artificial lights. (Note that visible lights also contain IR signals.) The ambient light could be so strong that the useful signals are completely overwhelmed. In order to isolate the useful light signals, we make the LED lamp switch on and off with a specified frequency using a low-end microcontroller. We then use FFT and inverse FFT to extract the signal strength at a particular frequency. Figure 2 shows a sequence of raw measurements of IR intensity and

1. The ISL29023 is an integrated ambient and infrared light to digital converter [22]. The same family of sensors are also found on other phones such as Motorola XT882.

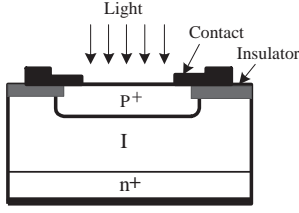


Fig. 4: The PIN structure of a photodiode.

the FFT result. In this test, the IR LED lamp flashed at a frequency of 65 Hz, and the nearby fluorescent lamps at the standard 100 Hz, with daylight imposing a strong intensity on the sensor with reading about 850, an order of magnitude higher than the lamp's effect on the sensor. Two spikes corresponding to the IR lamp and the fluorescent lamps can be clearly identified from the figure, which allows us to recover the intensity of the IR signal faithfully. In the following, when we say a light signal sensed by a light sensor, we mean the signal after the FFT processing.

The model for light intensity, or receive signal strength (RSS), is similar to a conventional light propagation model (e.g., the model in [44] or the Lambertian model [17]), with a focus on its stability in a realistic environment. The RSS, denoted by s , on a light sensor is mainly determined by three factors: the distance of light sensor to the light bulb d , the incident angle μ of light, and the emitting angle ω . It is well known that light intensity attenuates with increasing distance d according to an inverse square law. The incident angle μ plays an important role here, due to the working principle of the photodiode, which generates current under the striking of photons. When the flat contact layer is not perpendicular to the light, the energy with which the photons strike the contact layer decreases, and thus the received light energy drops; see Figure 4 for an illustration. Normally, the larger the deviation to the perpendicular orientation, the more loss to the light intensity [22]. Finally, s decreases with increasing ω , following the characteristics of light emitting diodes that behave in the same way. We call the direction with $\omega = 0$ the *central ray*. Furthermore, we say that the lamp is *vertically oriented* when the central ray is vertical, and *horizontally oriented* when the central ray is horizontal. Figure 3 shows the RSS model of a vertically oriented lamp, in which the tilted rectangle represents the sensor's surface, called its *sensing face*.

We need to determine three functions that respectively represent the influences of the three factors on RSS.

- $f_d(d)$, representing the impact of d on s , is obtained by varying d while fixing $\mu = \pi/2$ and $\omega = 0$, that is, making the sensing face perpendicular with the central ray.
- $f_\mu(\mu)$, representing the impact of μ on s , is obtained by varying the angle of the sensing face at a fixed d , with $\omega = 0$.
- $f_\omega(\omega)$, representing the impact of ω on s , is obtained

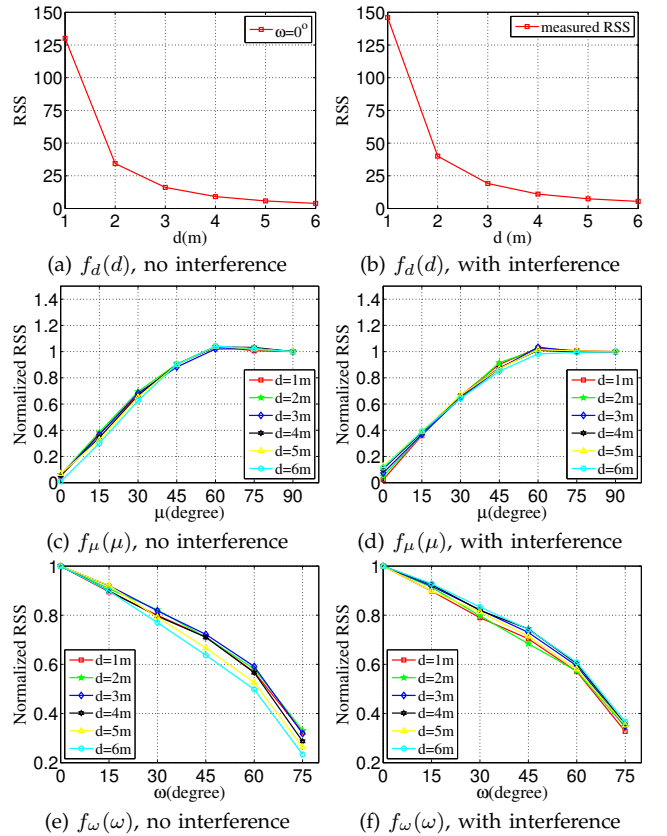


Fig. 5: The light sensor's reading as a function of d , μ , and ω in two scenarios, for the IR lamp.

by moving the sensor along a circle while keeping $\mu = 0$, that is, making the sensing face perpendicular with the emitting ray.

In fact, $f_d(d)$ captures the light signal's propagation law, $f_\mu(\mu)$ depends on the physical nature of a photodiode (at the receiver side), and $f_\omega(\omega)$ reflects the optical properties of the lamp's cover (at the transmitter side). The light intensity function is then modeled as:

$$s = f_d(d) \cdot f_\mu(\mu) \cdot f_\omega(\omega). \quad (1)$$

Interference-free scenario. First, we examined the property of the light sensor in a dark room at nighttime, where no ambient light is present. The first column of Figure 5 shows the impacts of the three factors, d , μ , and ω , on the RSS. It can be seen that $f_d(d)$ quite closely follows the well-known inverse square law for light intensity. (Small errors exist between the practical measurement and theory due to the physical properties of a photodiode, such as responsivity, dark current, etc [22]. These could be accounted for by calibration, but are ignored in our current design.) We can also see that $f_\mu(\mu)$ decreases with μ with fairly high predictability. The trends can be roughly captured by a sin function. For $f_\omega(\omega)$, the trend is also very deterministic, which can be modeled with a polynomial function.

Impact of ambient lights. This set of experiment was conducted in the morning, when the daylight imposed

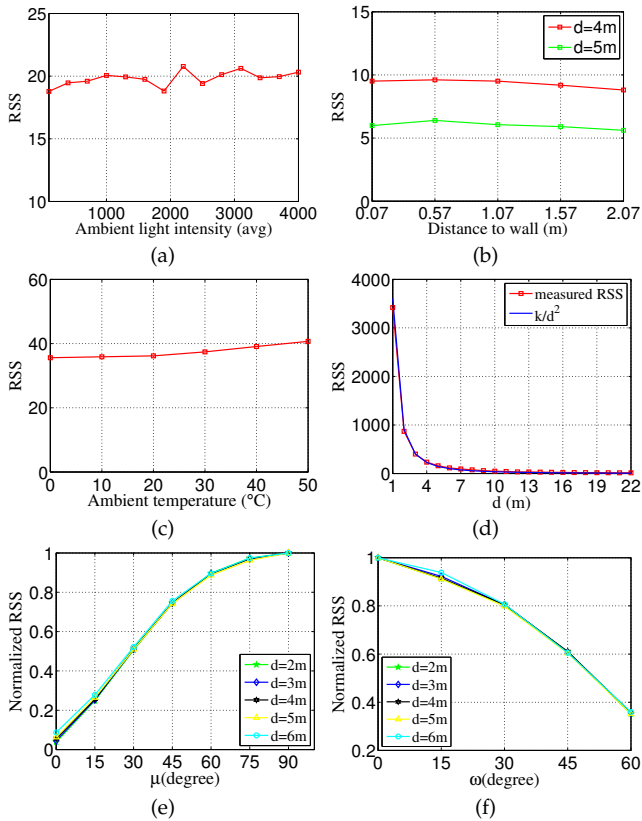


Fig. 6: Properties of a light sensor under various conditions. (a) Sensitivity to ambient light intensity. (b) Sensitivity to light reflection. (c) Sensitivity to ambient temperature. (d) Sensitivity to d under the visible light lamp. (e) Sensitivity to μ under the visible light lamp. (f) Sensitivity to ω under the visible light lamp.

an IR intensity reading of 800 on the sensor. In addition, three fluorescent lamps were turned on, emitting periodic IR signals with frequency 100 Hz. The intensity of ambient IR light was strong enough to overwhelm the RSS from the lamp at a distance of a few meters, however the frequency domain treatment can successfully extract the component of light intensity that we are interested in. The second column of Figure 5 shows the impacts of the three factors, d , μ , and ω , on the RSS. It can be seen that the results in both interference and interference-free environments are quite consistent, with differences normally within 10% of each other.

Figure 6(a) shows the impact of ambient light intensity as experienced by the sensor at different times (e.g., nighttime and daytime) and at various places in a room. The maximum value 4000 corresponds to the RSS near an open window at noontime of a sunny day. It can be seen that the extracted IR intensity of the LED lamp remains relatively stable, with a standard deviation as small as 0.58.

Impact of light reflection. This experiment examines how light reflection from surrounding objects affects the RSS. In a dark room, we kept the lamp horizontally oriented, with its central ray parallel to a wall and the floor, and vary the ray's distance to wall. The light sensor was placed at a certain distance from the lamp

with sensing surface perpendicular to the central ray. Figure 6(b) shows how the RSS changes with the distance to wall. It can be seen that the RSS experiences only insignificant changes. In our daily life, most materials (except glasses, polished metals, etc) give no more than a few percent specular (i.e., mirror-like) reflection [5]; that is, most of the light, upon hitting the surface of an object, is scattered in all directions, leaving only a small portion of reflected energy on the sensor. This explains the robustness of the RSS against wall reflection.

Impact of ambient temperature. Figure 6(c) shows how the RSS changes with ambient temperature. The low temperatures were produced by placing ice cubes around the sensor, and the high temperatures were generated by blowing at the sensor using a hair drier. We can see that the RSS increases with temperature, which agrees with the property of the photodiode reported in [22]. The trend is very mild, suggesting that only small errors are introduced by the temperature factor. In addition, the trend is monotonic, so the error could be compensated for with simple calibration.

High power LED lamp. We repeated the above experiments with the visible light lamp. Figure 6(d) shows the relationship between d and RSS, which closely matches the baseline curve of function k/d^2 . Due to the much increased power, the lighting range extends to nearly 30 meters, and for the same d , the RSS is much higher than with the IR lamp. In this test, the lamp was horizontally oriented and placed within a narrow corridor (about 2m wide) surrounded by wall, floor, and wooden boards, which presented complex conditions for light reflection. Compared to the low power IR lamp, the increased power causes more noticeable reflection effect. However, the variability is still below around 10% of the baseline. In a practical system, the lamps will be hung on ceilings and sensor mostly oriented upward, so the sensor is unlikely to be exposed to as strong reflection. It is thus reasonable to assume that the reflection effect does not fundamentally invalidate our RSS model in typical environments.

Figures 6(e)(f) show that the two functions $f_\mu(\mu)$ and $f_\omega(\omega)$ remain highly deterministic and consistent at different positions, though their particular forms differ from those of the IR lamp, due to the different photoelectric effects of the light sensor under IR and visible lights, and also because of the different scattering effects of the lamp covers.

3 LIGHT POSITIONING PRINCIPLE

In this section we describe two principles of light sensor positioning, one called *Multi-Face Light Positioning* (MFLP), which is our emphasis, and the other following the classic trilateration method.

The basic idea of MFLP is to have three (or more) properly oriented sensors to collect signal strengths as well as the sensors' orientation measures. Along with

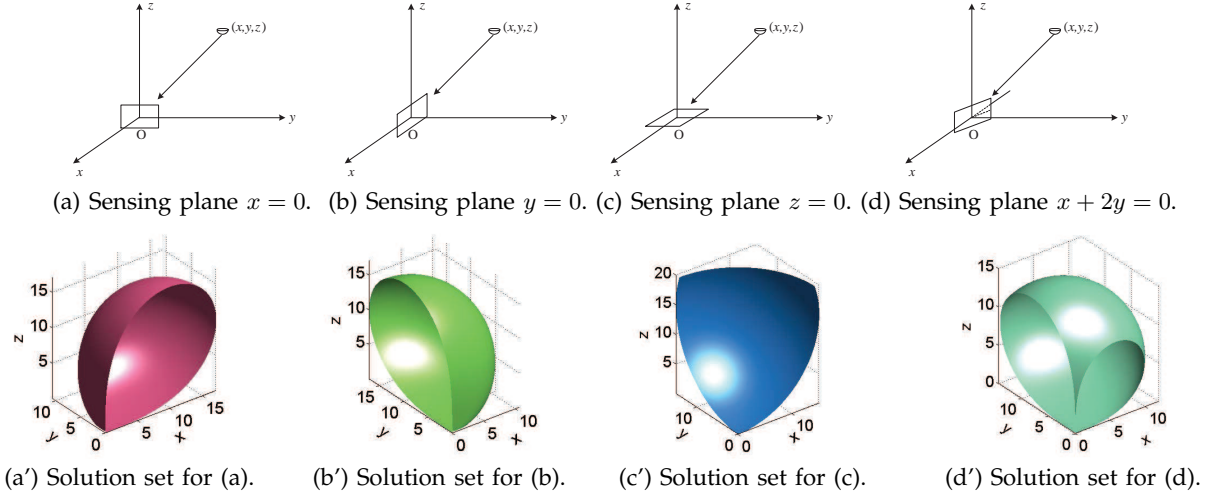


Fig. 7: The solution sets corresponding to different sensing faces.

the pre-defined RSS model, the measured data provides sufficient spatial constraints to locate the receiver. We call the top contact layer of the photodiode the *sensing face* of a light sensor, and the plane containing it the sensor's *sensing plane*.

3.1 Multi-Face Light Positioning

Assume the considered sensing face is centered at the origin $O = (0, 0, 0)$, and the point source of light is located at $X = (x, y, z)$, where $x > 0, y > 0, z > 0, \mu \in (0, \pi/2), \omega \in (0, \pi/2)$. The corresponding sensing plane has the form $Ax + By + Cz = 0$, where A, B, C are determined by the sensor's tilt and heading. Then, the distance between X and O is

$$d = \sqrt{x^2 + y^2 + z^2},$$

and the distance between X and the sensing plane is

$$d' = \frac{|Ax + By + Cz|}{\sqrt{A^2 + B^2 + C^2}}.$$

Following Eq. 1, let $f_d(d) = k/d^2$, $f_\mu(\mu) = \sin(\mu) = d'/d$, and $f_\omega(\omega) = f_\omega(\arccos(z/d))$, where $f_\omega(\cdot)$ is a monotonically decreasing function of ω (hence z). Therefore,

$$s = \frac{k}{d^3} \frac{|Ax + By + Cz|}{\sqrt{A^2 + B^2 + C^2}} f_\omega\left(\arccos \frac{z}{d}\right). \quad (2)$$

where $d = \sqrt{x^2 + y^2 + z^2}, x > 0, y > 0, z > 0, k > 0$, and s is a real number between 0 and some maximum reading value $s_m > 0$.

Theorem 1: When no measurement errors occur, three linearly independent sensing planes that pass through the origin and that satisfy the RSS model as specified by Eq. 2 determine a unique solution of $X = (x, y, z)$.

The system of equations generated by the mentioned three sensing plane is a high-order and nonlinear one, whose properties are in general not easy to obtain. Fortunately, the structure of A, B, C is simple enough to enable reduction among the equations, which makes

it possible to establish an exact relationship between the solvability and the linear independence property of (A_i, B_i, C_i) . The proof is provided in Appendix A.

Theorem 1 suggests that if we can create three linearly independent sensing planes on a receiver, and that these sensors can simultaneously 'see' the light source (i.e., in line of sight), then one can determine a position of the light source. With a bit of coordinate transformation, we can determine the position of the receiver provided the position of the light source.

When measurement errors exist, three linearly independent sensing faces may not lead to a solution. In this case, what we look for is a least square solution that minimizes the sum of the squares of the errors between each measured s and the calculated s from the corresponding equation.

3.2 Why Linear Independence of Faces

Since the geometric structure of the problem is not immediately intuitive, we now give a hypothetical example of MFLP to illustrate the necessity of the faces being linearly independent, which provides a key guideline for our system design. For the purposes of demonstration, we assume an simplified RSS model, in which $f_d(d) = 1/d^2$, $f_\mu(\mu) = \sin(\mu)$, and $f_\omega(\omega) = \cos(\omega)$. Then Eq. 2 can be rewritten as

$$s = \frac{z|Ax + By + Cz|}{\sqrt{A^2 + B^2 + C^2}(x^2 + y^2 + z^2)^2},$$

where $x > 0, y > 0, z > 0$.

Consider four sensing faces centered at the origin, whose sensing planes are $x = 0, y = 0, z = 0$, and $x + 2y = 0$, as shown in Figures 7(a)(b)(c)(d), respectively. The lamp is located at $X = (10, 10, 10)$ and imposes light intensity s_1, s_2, s_3 , and s_4 on the sensors, respectively. Given the known position of the lamp, the theoretical light intensities should be $s'_1 = s'_2 = s'_3 = 1/900$, and $s'_4 = 1/300\sqrt{5}$. Assume no errors occurring from the light

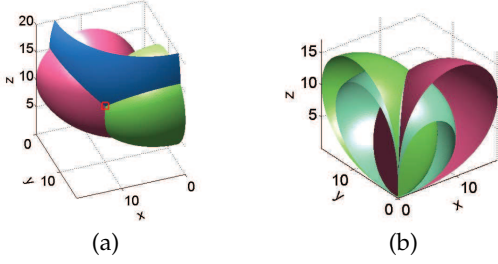


Fig. 8: The uniqueness of position solution. (a) The solution sets for the three sensing faces $x = 0, y = 0, z = 0$ intersect at a single point (red box). (b) The solution sets for the three sensing faces $x = 0, y = 0, x + 2y = 0$ intersect at a curve (partly shown).

propagation and measurement processes, the RSS seen on the sensors should be $s_i = s'_i$.

Now we choose the first three sensing faces, $x = 0, y = 0, z = 0$, which are *linearly independent*. These faces lead to a system of equations $h \cdot z / (x^2 + y^2 + z^2)^2 = 1/900$, where $h = x, y$ or z . Each of these equations will generate a solution set, as depicted by the curved surfaces in Figures 7(a)(b)(c), respectively. Figure 8(a) shows the intersection of these three solution set. It turns out that these surfaces intersect at a single point $(10, 10, 10)$, which matches the true location.

Next, consider an alternative set of three sensing faces, $x = 0, y = 0, x + 2y = 0$, which are *linearly dependent*. Figure 8(b) shows the intersection of their corresponding solution sets. Different from the first case, these sets do not intersect at a single point, but instead produce a curve segment (only partly shown due to blocking of surfaces), meaning infinitely many valid solutions for the three sensing faces. This comparison shows why linear independence of the sensing faces is necessary for unique solution of positioning.

3.3 MFLP vs. Trilateration

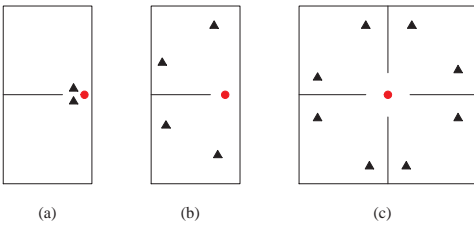


Fig. 9: Trilateration requires many more lamps than MFLP does for a full coverage of the environment. Small triangles and red dots represent the lamps. In all cases, MFLP needs only a single lamp (red dot).

The trilateration method assumes a single sensor, with three (or more) lamps as position references [17]. To reduce unknowns, the sensing face is assumed to be placed horizontally. Assume the sensor is located at (x, y, z) , and there are three non-collinear lamps at distinct positions $(x_i, y_i, z_i), i = 0, 1, 2$, then the following system of equations can be established with which one can solve for the solution

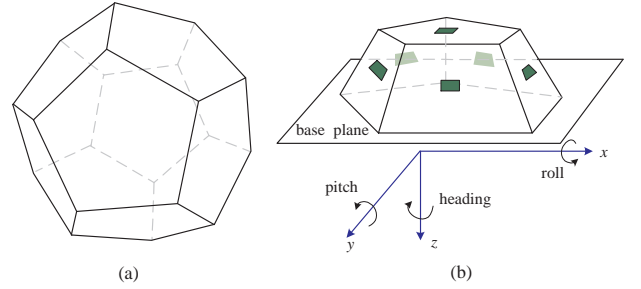


Fig. 10: (a) Dodecahedron (conceptual model). (b) Half dodecahedron (implementation model) on which six light sensors, represented by green blocks, are installed.

$$\frac{k}{d_i^3} \cdot |z - z_i| \cdot f_\omega \left(\arccos \frac{z - z_i}{d_i} \right) = s, \quad (3)$$

where $d_i = \sqrt{(x - x_i)^2 + (y - y_i)^2 + (z - z_i)^2}$, $k > 0$, and s is the RSS.

While simplifying the design at the receiver side, trilateration shifts cost to the transmitter side. In theory, trilateration requires three times as many lamps as MFLP does. In practice however, the difference can be much higher. Figure 9(a) shows a scenario where two adjacent rooms share a wall and a relatively narrow gate. With trilateration, every point needs to see at least three lamps. For a minimum deployment cost, the three lamps could be deployed near the gate. However, trilateration further requires the lamps not be close by or collinear, or huge errors or position ambiguities may arise. This makes it necessary to place at least two additional lamps in each room (Figure 9(b)). Thus, trilateration ends up using five times as many lamps as used by MFLP. Figures 9(c) further shows a case where trilateration needs nine times as many lamps. In a real-world environment, obstructions may appear in different forms, but a similar comparison can be drawn between the two approaches in terms of light coverage and deployment density.

Therefore, when the positioning system is deployed from scratch and lamp deployment cost is a primary concern, the MFLP approach appears to be a more economical solution. On the other hand, when there already exist dense lamps (as in some public places such as shopping malls, airport terminals, etc) that can be re-used for positioning, and when a small size of receiver is preferred, the trilateration approach might be the choice. Since the trilateration approach is well studied and understood, we shall concentrate on the MFLP approach in the following sections.

4 LIPS RECEIVER DESIGN

In this section we describe a design for a dedicated LIPS receiver based on the MFLP principle.

4.1 Number and placement of light sensors

We say that a sensor face can ‘see’ a point p if there is a line of sight between p and all points on that

sensing face. Although a receiver can be positioned with only three sensors at particular places, visibility of those sensors to a lamp may be lost when the receiver is moving around. Thus, we need more than three sensors to support positioning everywhere (assuming full coverage of light on the ground). Toward that goal we need to answer two questions: how many sensors do we need, and how to place them?

For implementation convenience, we focus on a regular polyhedron framework on which the sensors are to be placed. Our choice is a dodecahedron model, as shown in Figure 10(a), in which 12 regular pentagonal faces each host a sensor. This model possesses three desirable properties:

- 1) *Tri-face visibility*: Any point p in the space beyond a short distance from the dodecahedron can see at least three faces of that dodecahedron;
- 2) *Tri-face linear independence*: Any three of the faces seen by the above mentioned point p are linearly independent;
- 3) *Minimal faces*: Among all regular polyhedra, a regular dodecahedron has the fewest faces that satisfy the above two properties.

Theorem 2 gives a more formal description of the Tri-face visibility property. The theorem can be proved with basic trigonometric operations and is thus omitted here.

Theorem 2: Assume the edge length of a regular dodecahedron centered at the origin is a , then for an arbitrary point at a distance D from the origin, at least three faces of the dodecahedron can see it if

$$D \geq \left(\sqrt{1 + \frac{2}{5}\sqrt{5}} + \frac{1}{2}\sqrt{\frac{5}{2} + \frac{11}{10}\sqrt{5}} \right) a \approx 2.49a.$$

In LIPS, a is at the order of a few centimeters, so the dodecahedron faces can be viewed as roughly passing through the origin from the perspective of the lamp. Theorem 2 means that if we place 12 sensors along the faces of a regular dodecahedron, then the receiver can always be positioned, regardless of the receiver's orientation.

The tri-face linear independence property can be easily verified by examining the plane coefficients of the faces of a dodecahedron. Finally, the minimal faces property can be proved by excluding the regular polyhedra with fewer faces. For example, a cube-aligned placement of sensors may be able to position a receiver sometimes, as demonstrated in Section 3.2, but it is easy to pick a point in the space from which only a single face is visible.

To further reduce the cost, we make a simplification to the conceptual model by employing only a half of the dodecahedron, which is fixed on a *base plane* (Figure 10(b)) of the receiver. This way we need only six sensors attached to the six exposed faces. This does not affect the positioning ability as long as lamps are hung above at ceilings and the half dodecahedron is oriented upward.

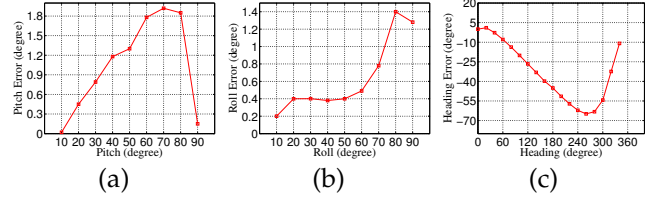


Fig. 11: Errors of pitch, roll, and heading, produced by an acceleration sensor and a magnetic sensor.

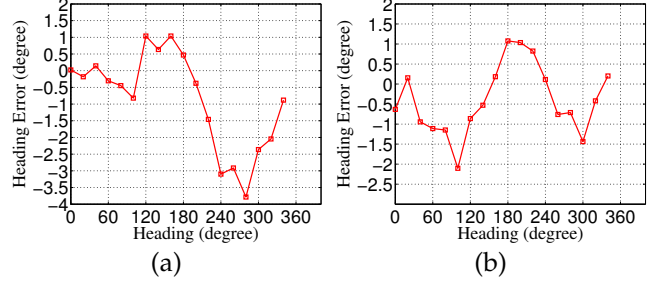


Fig. 12: Heading errors under auto-calibration. (a) Half dodecahedron calibration. (b) Circular calibration.

4.2 Sensing plane coefficients

The coefficients of a sensing plane, namely A , B and C , are obtained from acceleration and magnetic sensors. Following the aircraft convention, we use three attitude angles, *pitch*, *roll* and *heading*, to describe a receiver centered coordinate system. Figure 10(b) shows the coordinate system, in which x , y and z are defined as forward/right/down based on the right-hand rule, and the three attitude angles are referenced to the local horizontal plane which is perpendicular to the earth's gravity.

Denote the pitch, roll, and heading by θ_p , θ_r and θ_h . The first two angles can be obtained with an acceleration sensor, which produces three components of the gravity along the x , y , and z axes. Comparing these components against the acceleration of gravity can give the two angles. Figures 11(a)(b) show that these two angles can be measured with accuracy to 2 degrees. A standard way of obtaining θ_h is using an electronic compass. However, a compass is very susceptible to interferences. To confirm this, we rotate a compass containing a magnetic sensor and obtain the heading error with respect to a calibrated electronic compass. Figure 11(c) shows that the raw measurement of heading can vastly deviate from the true value, with errors up to 60 degrees. We discuss how to calibrate a compass in the next section.

The three angles θ_p , θ_r and θ_h entirely determine the orientation of the sensing plane, thus the coefficients A , B and C . We use the rotation matrix [29] to convert the angles to A , B and C .

4.3 Accurate heading measurement

Magnetic sensor is known to be vulnerable to environmental interferences, because the Earth's magnetic field is a weak signal. A mobile receiver carried around

may experience distinct distortion patterns at different locations. This property is exploited by [13] to enable receiver positioning, but causes trouble to a system that needs accurate heading information in real time. The general approach to auto-calibration of a compass requires multiple types of sensors to provide redundant measurements to correct heading errors. The redundant information can be from optical trackers [14], inertial sensors [16], visual analysis [47]. In our context, these techniques are unsuitable because they either involve extra infrastructure or does not provide bounded errors in a long period of time [16].

LIPS uses a new auto-calibration technique for heading measurement. The idea is inspired by the standard manual calibration method, in which sufficient 3D rotation or several full round 2D rotations are performed to collect magnetic field strengths. Ideally the readings along the three axes should form a sphere centered at the origin. In practice, environmental interferences will distort the sphere, resulting in a tilted ellipsoid [33]. Given a set of manually collected magnetic field data, the least square fitting method can be used to discover the parameters of the ellipsoid, which are then applied to correct errors of raw measurements.

LIPS avoids the manual operation by using multiple magnetic sensors that are placed in a spherical or circular layout. These sensors can produce a number of magnetism readings at once, thus provide a sparse sampling of the needed magnetic data. We have experimented with various numbers of sensors and found six sensors strike an acceptable balance between measurement accuracy and cost. The spherical layout is approximated with a half dodecahedron. In this experiment, we manually collected the readings along the six faces using the same magnetic sensor. Figure 12(a) gives the heading errors with the half dodecahedron calibration at the same position that produced the errors in Figure 11(c). We can see that the original error of 60+ degrees is now reduced to around 4 degrees.

The six magnetic sensors can also be placed in a circular pattern when the receiver is placed horizontally. Before performing the collective calibration, the various magnetic sensors are individually calibrated to achieve a consistent effect by rotating the board in an interference-free environment and collecting the readings from individual sensors. On a horizontal plane, the reference model of the magnetic field strength should be an ellipse instead of an ellipsoid, which means that the fitting process deals with fewer parameters. As a result, the heading accuracy after calibration will be more accurate than with the half dodecahedron calibration. Figure 12(b) shows that the heading error has now drops to around 2 degrees.

5 PROTOTYPE IMPLEMENTATION

We have implemented a dedicated LIPS receiver and a smartphone based receiver. This section details the implementation.

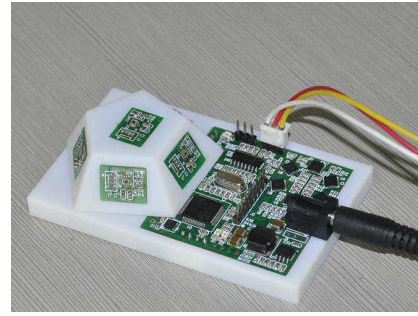


Fig. 13: The CompEye receiver, sized 9.5 cm×5.7 cm. The six light sensors are embedded in a half-dodecahedron model, and are connected to the main board from within the model.

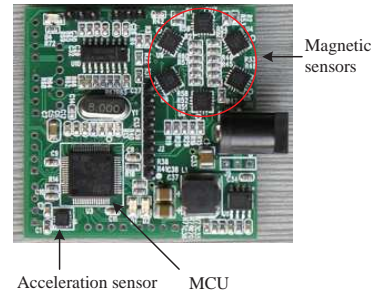


Fig. 14: Main board of LIPS receiver, sized 5 cm×5 cm.

5.1 The CompEye receiver

Figure 13 shows the dedicated LIPS receiver, called CompEye (compound eye), for position tracking applications. The receiver consists of two parts: the main board, shown in Figure 14, and the light sensing component. The former is a circuit board integrating an STM32F103RC microcontroller (MCU), six AKM8975 magnetic sensors, and an ST LIS33DE accelerometer. The magnetic sensors are arranged along a circle for heading calibration. The light sensing component comprises six ISL29023 light sensors fixed on the surfaces of a half-dodecahedron model; each sensor is linked to the main board individually. In the prototype design, the receiver is powered by an external battery, and uses a wireless serial adapter for transmitting data to a server. In the future, the power module will be replaced by a lithium battery like one used by a mobile phone, and the WiFi module will be integrated into the main board.

The MCU samples each light sensor at a rate of 640 Hz, and performs FFT transformations to extract the light intensities of surrounding light sources (identified by peaks in the frequency domain). The MCU also samples each magnetic sensor at a rate of 20 Hz, and performs calibration, first individually and then collectively, to obtain the current heading of the receiver. The tilt and pitch are calculated from the reading of the acceleration sensor. The MCU maintains a sliding-window for each sensor, and performs the above calculations every Δ seconds (e.g., $\Delta = 0.3$), and sends the light intensities, heading, title, and pitch to the sever. The sever stores a digital map of the physical environment and of the deployed lamps, with which it solves for the receiver's

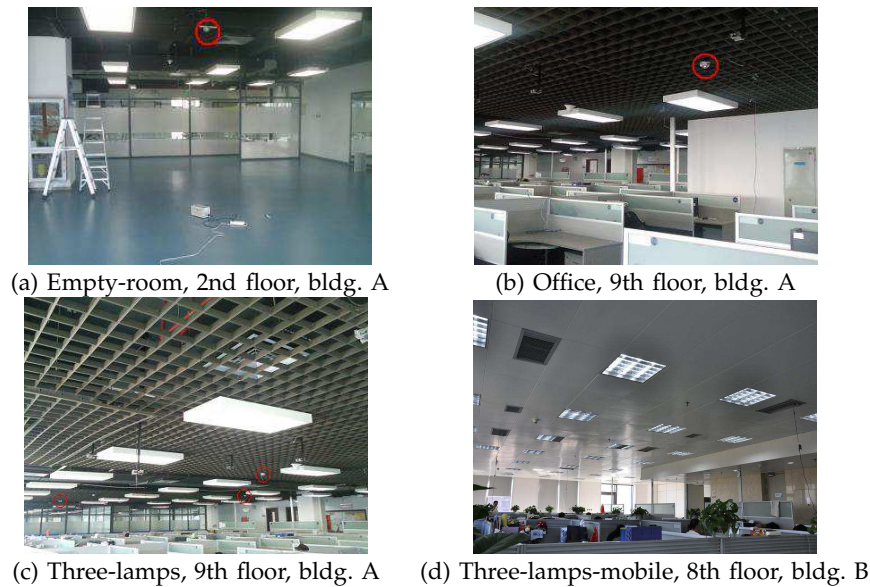


Fig. 15: Experimental scenarios for LIPS prototype. (a) Empty-room: An empty room with a single IR LED lamp. (b) Office: An office environment with a single IR LED lamp. (c) Three-lamps: An office environment with three IR LED lamps flashing at rates 55 Hz, 65 Hz, and 75 Hz. (d) Three-lamps-mobile: Another office environment with three IR LED lamps flashing at rates 55 Hz, 65 Hz, and 75 Hz; the receiver is being moved.

position using a least square optimization algorithm.

5.2 Smartphone

We used a Samsung Omnia II GT-I8000 smartphone to evaluate the design. We installed an Android system with Linux kernel 2.6.32, which allowed us to configure the light sensor in the driver to sense infrared light instead of the default visible light.

After the configuration the phone can give correct readings of IR intensity, as verified against a stand-alone sensor. However, under periodical sampling, the sequence of readings produced by the Android interface contains many uneven gaps in time, making the frequency analysis difficult. This is because the OS kernel contains a routine to smoothen sensed data and filter out readings with only small changes. This treatment seriously affects frequency analysis. We modified the `input_defuzz_abs_event()` function in `input.c` to disable the smoothing procedure for the light sensor, and rebuilt the kernel, after which the sensor started working normally.

The smartphone can be positioned with the trilateration method, since there is only one sensor. We evaluate its effectiveness in the next section.

6 EXPERIMENTS

We conduct experiments in three static scenarios and one mobile scenario. We mainly consider IR LED lamps as they can be incrementally deployed without interfering with the existing lighting design of an environment.

- 1) In this scenario, labeled *Empty-room* (Figure 15(a)), an IR LED lamp is hung on the ceiling of an empty room, where there is little obstruction and the floor

is reflective. We selected 50 points of interest with rough uniformity across the sensing area for test.

- 2) The second scenario, *Office* (Figure 15(b)), is a crowded office environment with dense cubicles, which create complex conditions for light reflection. Again a single IR LED lamp was used, and 50 points, both on the floor and on the desk, were selected for positioning.
- 3) The third scenario, *Three-lamps* (Figure 15(c)), is similar to the second one, except that there were three lamps used that flash at rates 55 Hz, 65 Hz, and 75 Hz. We deliberately made the lamps' sensing areas overlap more than necessary to examine the effect of increased face exposure to light signals. In this scenario, 98 points of interest were chosen, with a bias to the overlapped areas. Throughout the test, the receiver had its base plane placed horizontally on the floor or the desk.
- 4) The fourth scenario, *Three-lamps-mobile* (Figure 15(d)), consists of three lamps placed in a similar layout as in the *Three-lamps* scenario. This experiment is conducted in a different building which creates more diversity of experimental conditions. The receiver is moved along three straight lines while position data is collected. We compare the collected traces against the ground truth to check the system's mobile performance.

6.1 Position accuracy

CompEye receiver. When there is no obstruction, a LIPS receiver can normally find at least three faces visible to a lamp in range; normally it can find four. We have found that the additional face generally does not improve the positioning result, because of its small incident angle μ

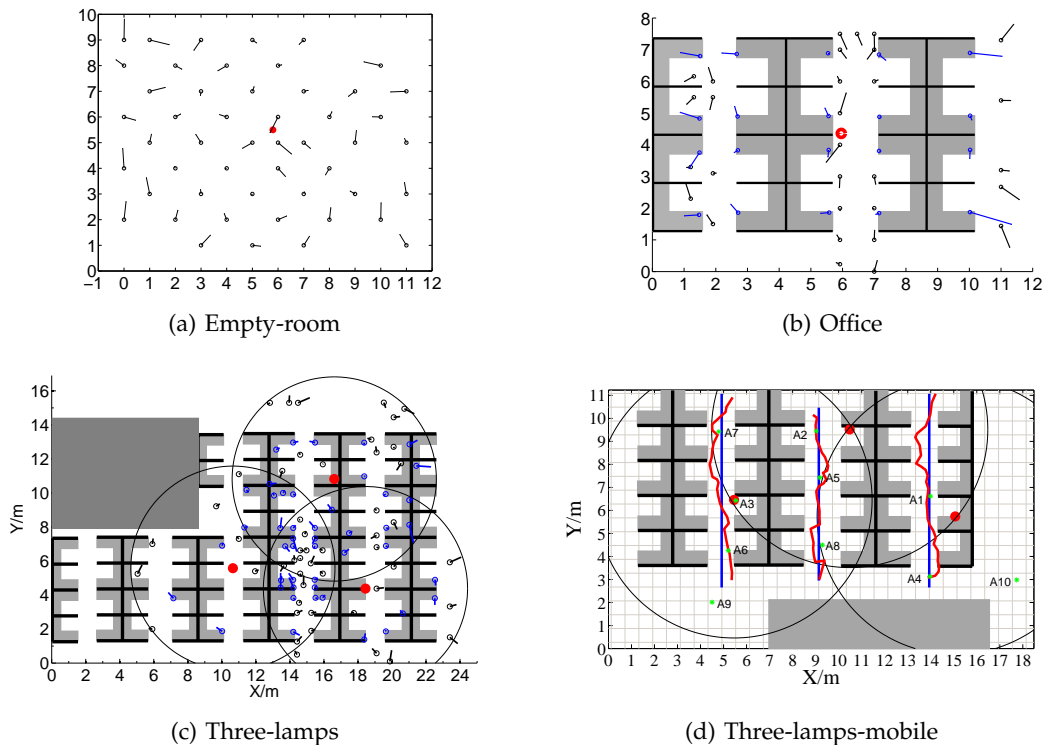


Fig. 16: Positioning results of a CompEye receiver. Gray areas represent desks or obstacles, red dots lamps, and small circles test spots. (a) Empty-room, size 12m×10m, (b) Office, size 12m×10m, (c) Three-lamps, size 24m×16m. (d) Three-lamps-mobile, 18m×12m.

Test cases	Error statistics (m)			
	Median	Mean	Max	Stdev
Empty room, CompEye	0.36	0.39	0.79	0.20
Office, CompEye	0.33	0.36	0.73	0.20
Three-lamps, CompEye	0.32	0.32	1.08	0.20
Three-lamps, smartphone	0.39	0.44	1.05	0.29

TABLE 1: Position error statistics in different scenarios. Note that the smartphone case assumes a trilateration method, which requires denser deployment of lights than the other cases.

that produces a very low RSS, potentially introducing increased errors from the tail of $f_d(d)$. Therefore, for a particular lamp, we always choose the three faces with the strongest RSS for position calculation. When the receiver is covered by two or three lamps, it chooses the lamp that imposes a stronger average RSS (over three faces) for positioning.

Figures 16 (a,b,c) show the maps of the various environments as well as the positioning results. In the figures, the red dots represent lamps, small dots true positions, and a line segment connects a true position to its corresponding result of positioning. The length of a line segment is thus proportional to the positioning error. In all cases, the median and average errors are below 0.4 meters (Table 1). The consistence is also reflected in the small standard deviation. Notice that quite different environmental conditions, including floor/wall reflection, ambient temperature and ambient light intensity (implied by time of day), etc, are contained in these scenarios. These variations cause unnoticeable difference in the positioning accuracy, suggesting that LIPS is robust

to environmental differences.

Figure 16(d) shows the mobile performance of the LIPS receiver. In this experiment, the receiver is placed on a small cart moving along the central lines of the three corridors. The positions of the receiver are generated at an approximate interval of 0.3 seconds. The red lines show the position traces of the receiver; the cells are of size $0.6\text{m} \times 0.6\text{m}$. It can be seen that the positioned traces stay within 0.6m of the true trace lines, with an average much lower than 0.6m .

Smartphone. We also experimented with the trilateration method using a smartphone. A total of 33 points were randomly picked with rough uniformity in the intersection area of the three lamps. The phone was horizontally placed when collecting the RSS. The error statistics are given in the last row of Table 1. It can be seen that the average error now goes up to 0.44 meters, which is worse than those of the CompEye receiver. This is mainly because of the absorption of light by the phone screen and the blocking of phone body, especially when the incident angle is small.

6.2 Position stability

It is normal for a positioning system to generate position oscillation due to instability of signal propagation, environmental interferences, and various errors in the system. The degree of oscillation is an important impact factor for user's experience. Though multiple position samples could be collected to increase stability, in delay sensitive applications oscillation is still likely to cause feelings of uncertainty and visual discomfort.

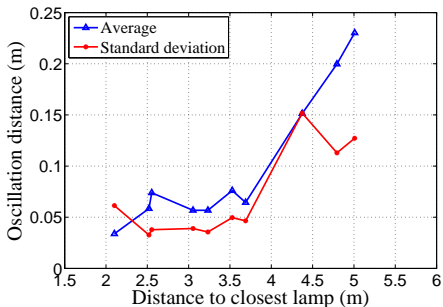


Fig. 17: Oscillation distance of ten test spots in the Three-lamps-mobile scenario.

Given a spot in the field, we define the positioning system’s *oscillation distance* as the average distance of the produced position samples from the centroid of those samples. In the Three-lamps-mobile scenario, we choose 10 test spots A1, A2, ..., A10 with different distance to their closest lamps, and for each test spot, approximately 300 position samples are collected to obtain an average and a standard deviation. Figure 17 depicts the results against the distance to closest lamp. First, it can be seen that the averages remain below 0.25m, indicating that the positions are quite stable. Second, the oscillation distance generally increases with the spot’s distance to closest lamp, due to the increased signal/noise ratio at a larger distance.

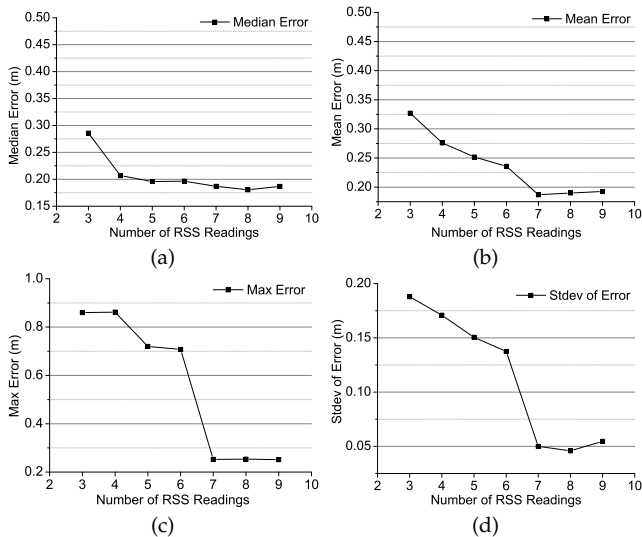


Fig. 18: Positioning errors of the CompEye receiver for various number of RSS readings.

6.3 Sensitivity analysis

Impact of lamp density. In the three-lamps scenario, there are 98 points for testing, out of which 61 are covered by a single lamp, 30 by two, and 7 by three. Thus, a receiver may have more than three faces visible to a lamp, and a sensing face may see multiple lamps. Let m denote the number of RSS readings a receiver collects.

Since the receiver records only three highest RSSs with respect to a lamp, and there are only three lamps, we have $3 \leq m \leq 9$. In fact, each RSS will result in an equation 2, and we have already shown that three such equations can lead to a position. Here we want to see if using more than three RSSs will be beneficial. To that end, we pick m' highest RSSs for each point p , where the receiver has $m \geq m'$, and establish an system of m' equations, by which we solve for positions.

Figure 18 shows how position errors are affected by the number of RSS readings, m . It can be seen that in general, increasing m results in improved accuracy, reducing average errors to below 0.2 meters. In particular, the maximum error and standard deviation of error drop quite sharply with m , suggesting the significant benefit of multiple lamps in reducing outliers and improving positioning stability. The declining trend starts flattening after $m > 7$, implying a limiting accuracy of around 0.19 meters under the present RSS model.

Note that the case of more than three faces provides a generalization of MFLP, which essentially mixes the principles of MFLP and trilateration.

Error sensitivity. In this test, we examine the sensitivity of positioning quality to two main sources of error: RSS error and heading error. We introduce artificial perturbations to the measured data, and then calculate position errors. For each RSS reading, a multiplicative perturbation $(1 \pm \epsilon)$ is applied, where $0 \leq \epsilon \leq 20\%$ is a parameter and the sign is chosen randomly. For each heading measurement, an additive perturbation $\epsilon_h \in [-10^\circ, 10^\circ]$ is applied. In our experiments, the fluctuation of both measures was rarely found to exceed half of the assumed ranges.

Figure 19 shows how positioning accuracy changes with the perturbations in the Office scenario. As expected, the average errors increase with larger perturbations. The increasing trend, however, is smooth and mild, having average errors well under 1 meter even for unrealistically large perturbations.

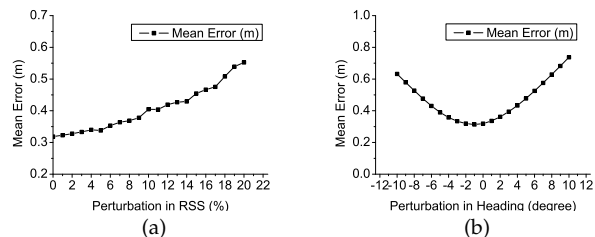


Fig. 19: Position errors changing with perturbations to RSS and heading.

7 DISCUSSION

Power consumption. The LIPS receiver consumes power mainly in three tasks: sensing, computation, and transmission. Each ISL29023 light sensor has a power overhead of $70\mu A \cdot 3.6 V = 0.25 mW$ in continuous sensing mode [22]; each magnetic sensor uses less than 0.2 mW at

20 Hz sampling rate, and a LIS33DE accelerometer uses less than 1 mW [35]. Overall, the sensing part accounts for less than 4 mW. The MCU and the networking module normally have much higher power consumption rate. However, their actual power consumption depends on the position sampling rate as specified by the application. The computation and transmission tasks can thus be performed with a low duty cycle to reduce power consumption.

In terms of power overhead by the sensing task itself, LIPS consumes merely 4 mW. It takes less than one second to obtain a relatively stable position from a cold start, which amounts to about 4 mJ energy. By contrast, a WiFi scan used by the WiFi-based positioning system consumes 0.55 J [20], which is two orders of magnitude higher than LIPS's cost.

Limitations. The current design of LIPS system does not support other forms of light sources. For example, our RSS model does not apply to the widely used tube-shaped lamps. In principle, the point-source based model should be extended to a line-segment model. We have done some preliminary experiments with LED tubes, and found that the RSS characteristics remain stable, though the relations between RSS and distance/angle become more complicated. This means that a geometry based positioning method is still possible, though its mathematical foundation needs further investigation.

Currently, the full scale range of an ISL29023 light sensor is set to 1000 lux. In a typical indoor environment (e.g., office lighting), the daylight's illuminance is less than 500 lux [2], which is well within the sensor's capability. However, the sensor quickly gets saturated under direct sunlight, for example in the glass-ceilinged atria of some modern buildings, making the receiver unable to position itself. This problem can be mitigated by raising the sensing range (to a maximum of 64,000), at the cost of reduced sensitivity or data resolution, which implies reduced positioning accuracy. For higher adaptability while retaining the accuracy, we will need to seek more powerful light sensors to work for more challenging circumstances.

8 RELATED WORK

Positioning principle. Most existing indoor positioning systems follow one of three basic principles: proximity detection, fingerprint matching, and trilateration/angulation. The proximity detection approach [28], [23] localizes a receiver simply with the positions of signal sources that can be sensed by the receiver. Fingerprint matching [48], [7] further employs signal strength to obtain more accurate positions. The last approach, trilateration/angulation, can produce highly accurate positions when ranging/angulation ability is available on the signal transmitter or receiver. Various methods such as time-of-arrival (TOA), time difference of arrival (TDOA), angle of arrival (AOA), and two-way sensing [21], can

be used to obtain distance or angle, based on which a position can be calculated.

LIPS follows a principle similar to the third one, with an important difference. In LIPS, the light sensor is simultaneously sensitive to distance and incident angle of light signal, yet there is no way to obtain either measure with the RSS alone, rendering the traditional trilateration and angulation methods inapplicable. In LIPS, only when several sensors' readings are collected can one solve for the receiver's position, without explicit knowledge of distance and angle.

Light signal based indoor positioning has been studied in a number of previous works; see for example [1], [4], [44], [43], [25]. The visible light communication (VLC) technology [4] uses cameras on mobile devices to capture flashing patterns from programmed LED lamps, whose positions are then used to estimate the user's position. The ByteLight solution [1] appears to follow a similar approach. The Pharos [17] system also uses light signal and is based on the classic trilateration method [17]. In [44], a positioning system is designed that uses a single transmitter and multiple receivers based on visible light produced by white LEDs. The multiple receivers are independent and thus the positioning principle behind fundamentally differs from ours.

Infrastructure dependence and deployment cost. Early indoor positioning systems use dedicated devices such as Bluetooth [28], RFID [23], or sensor nodes to realize positioning via proximity detection, but on the other hand require a relatively dense deployment of signal transmitters. Higher positioning accuracy is provided by more accurate ranging techniques such as a combination of radio and sound signals [26], Ultra Wide Band (UWB) technology [30], etc. These techniques require synchronization and coordination among signal transmitters or expensive devices, which greatly increase the overall cost.

A class of positioning techniques require little or no dedicated infrastructure. They use ambient signals such as cellular radio [39], FM radio [11], magnetism [13], ultrasound [8] to create position fingerprints. These solutions often provide only coarse grained positioning, for example at room level granularity [8]) or work for only special environments (e.g., steel rich buildings [13]). The most notable technique in this class is the WiFi RSS fingerprint based scheme [48], [7] (the WiFi scheme). It exploits pre-existing AP hotspots to create signal fingerprints. Depending on the density and placement of APs, the positioning accuracy varies.

Infrastructure cost depends not only on hardware investment, but also on human effort in site survey. The latter factor is a serious concern for fingerprinting based solutions, represented by the WiFi scheme. Recently researchers have proposed various schemes that use little or zero explicit human effort [27], [45], [42]. These techniques leverage inertial sensors on smartphones to automatically infer a user's real position while collecting

RSS data. While they represent significant advances toward low-cost deployment, the solutions are not generic, since they require the environments to possess special structural characteristics. When the indoor environment contains large free spaces (e.g., in a factory or a large warehouse), or has a symmetric layout, position ambiguity may arise which prevents exact positions from being inferred from the user's trace.

LIPS uses off-the-shelf LED lamps as signal sources, with a cheap microcontroller attached to each lamp to control flashing. On the receiver side, a dedicated receiver uses a number of light and magnetic sensors, each costing no more than a few US dollars.

Accuracy and stability. Different applications require different levels of positioning accuracy. For example, in-building pedestrian route guidance may work well with an accuracy to a few meters, while automated handling requires positioning accuracy within 1 cm [30]. The WiFi scheme mostly offers an accuracy of 1 to 3 meters, and is known to be instable in positioning quality, since the RSS at a fixed position varies significantly over time, and is sensitive to obstacle presence, receiver orientation, and type of device. Also the distinctiveness of fingerprints depends heavily on AP density [10]. It is reported that the same scheme can produce drastically different performance across different environments. For example, the classic RADAR scheme is found to generate median accuracies of 1.3m and 5m in a small and a large buildings, respectively [12]. An empirical study [38] shows that an algorithm can yield 5× worse accuracy than in its original test environment. LIPS is based on light intensity, which is relatively stable once separated from ambient lights, thus the positioning quality is better guaranteed than the WiFi scheme does.

9 CONCLUSION

We have presented a light intensity based positioning system, *LIPS*, for indoor environments. *LIPS* exploits ordinary lighting devices such as LED lamps as signal transmitters, and uses light sensors as signal receivers. Several light sensors on a receiver can jointly determine the receiver's position with the measured RSS. The main contribution of *LIPS* is that it explores a new way of indoor positioning, with fairly high accuracy and high stability. The design is fingerprint free, requiring little human intervention other than the establishment of an RSS model. In the future we will extend the design to more complex lighting environments.

REFERENCES

- [1] ByteLight. <http://www.bytelight.com/>
- [2] Lux. http://en.wikipedia.org/wiki/Lux#cite_note-9
- [3] Time Domain. <http://www.timedomain.com/>.
- [4] VLC for location, positioning and navigation. <http://visiblelightcomm.com/vlc-for-location-positioning-and-navigation/>
- [5] Diffuse reflection. http://en.wikipedia.org/wiki/Diffuse_reflection
- [6] M. Azizyan, I. Constandache, and R. Roy Choudhury. Surround-Sense: Mobile Phone Localization via Ambience Fingerprinting. In *MobiCom*, 2009.
- [7] P. Bahl and V. N. Padmanabhan. RADAR: An Inbuilding RF-based User Location and Tracking System. In *INFOCOM*, 2000.
- [8] G. Borriello, A. Liu, T. Offer, C. Palistrant, and R. Sharp. WALRUS: wireless acoustic location with room-level resolution using ultrasound. In *MobiSys*, 2005.
- [9] A. Carroll and G. Heiser. An Analysis of Power Consumption in a Smartphone. *USENIX Annual Technical Conference 2010*.
- [10] G. Chandrasekaran, M. A. Ergin, J. Yang, S. Liu, Y. Chen, M. Gruteser, and R. P. Martin. Empirical evaluation of the limits on localization using signal strength. In *6th Annual IEEE communications conference on Sensor, Mesh and Ad Hoc Communications and Networks*.
- [11] Y. Chen, D. Lymberopoulos, J. Liu, and B. Priyantha. FM-based indoor localization. In *ACM MobiSys*, 2012.
- [12] K. Chintalapudi, A. P. Iyer, and V. N. Padmanabhan. Indoor Localization Without the Pain. In *Mobicom*, 2010.
- [13] J. Chung, M. Donahoe, I. Kim, C. Schmandt, P. Razavi, M. Wise-man. Indoor location sensing using geo-magnetism. In *MobiSys*, 2011.
- [14] S. Gottschalk and J. Hughes. Autocalibration for Virtual Environments Tracking Hardware. *ACM SIGGRAPH 1993*.
- [15] A. Haeberlen, E. Flannery, A. M. Ladd, A. Rudys, D. S. Wallach, and L. E. Kavraki. Practical Robust Localization over Large-Scale 802.11 Wireless Networks. In *MobiCom*, 2004.
- [16] B. Hoff and R. Azuma. Autocalibration of an Electronic Compass in an Outdoor Augmented Reality System. *IEEE/ACM Intl. Symposium on Augmented Reality 2000*.
- [17] P. Hu, L. Li, C. Peng, G. Shen, and F. Zhao. Pharos: Enable Physical Analytics through Visible Light based Indoor Localization. *ACM Hotnets 2013*.
- [18] A. LaMarca, Y. Chawathe, S. Consolvo, J. Hightower, I. Smith, J. Scott, T. Sohn, J. Howard, J. Hughes, F. Potter, et al. Place lab: Device positioning using radio beacons in the wild. *Pervasive Computing*, 2005.
- [19] H. Lim, L. Kung, J. Hou, and H. Luo. Zero-Configuration, Robust Indoor Localization: Theory and Experimentation. In *Infocom*, 2006.
- [20] K. Lin, A. Kansal, D. Lymberopoulos, and F. Zhao. Energy-accuracy Trade-off for Continuous Mobile Device Location. In *MobiSys 2010*.
- [21] H. Liu, Y. Gan, J. Yang, S. Sidhom, Y. Wang, Y. Chen, F. Ye. Push the Limit of WiFi based Localization for Smartphones. In *ACM Mobicom*, 2012.
- [22] Intersil. The ISL29023 Datasheet. July 17, 2012.
- [23] L. Ni, Y. Liu, C. Yiu, and A. Patil. LANDMARC: Indoor Location Sensing Using Active RFID. In *WINET*, 2004.
- [24] D. Niculescu and B. Nath. Ad hoc positioning system (APS) using AOA. *IEEE INFOCOM*, 2003.
- [25] G. B. Prince and T. D. Little. A two phase hybrid RSS/AoA algorithm for indoor device localization using visible light. In *IEEE Global Communications Conference (GLOBECOM)*, 2012.
- [26] N. B. Priyantha, A. Chakraborty, and H. Balakrishnan. The Cricket Location-Support System. In *MobiCom*, 2000.
- [27] A. Rai, K. K. Chintalapudi, V. N. Padmanabhan, and R. Sen. Zee: zero-effort crowdsourcing for indoor localization. In *Mobicom 2012*.
- [28] B. Raffaele; D. Franca. Design and analysis of a Bluetooth-based indoor localization system. *Workshop on Personal Wireless Communications 2003*.
- [29] Rotation Matrix. http://en.wikipedia.org/wiki/Rotation_matrix.
- [30] Z. Sahinoglu, S. Gezici, I. Guvenc. *Ultra-wideband Positioning Systems: Theoretical Limits, Ranging Algorithms, and Protocols*. 2008.
- [31] S. Sen, R. R. Choudhury, and S. Nelakuditi. SpinLoc: Spin once to know your location. In *ACM HotMobile*, 2012.
- [32] S. Sen, B. Radunovic, R. R. Choudhury, and T. Minka. Precise Indoor Localization using PHY Layer Information. In *ACM HotNets*, 2011.
- [33] STMicroelectronics. Using LSM303DLH for a tilt compensated electronic compass, AN3192 Application note, 2010.
- [34] STMicroelectronics. STM32 MCU family – 32-bit Flash microcontrollers powered by ARM CortexTM – M3, May 2008.
- [35] STMicroelectronics. LIS33DE datasheet, April 2009.

- [36] S. Tarzia, P. Dinda, R. Dick, G. Memik. Indoor Localization without Infrastructure using the Acoustic Background Spectrum. In *ACM MobiSys*, 2011.
- [37] A. Thiagarajan, L. Ravindranath, H. Balakrishnan, S. Madden, L. Girod. Accurate, Low-Energy Trajectory Mapping For Mobile Devices. *Proc. of NSDI* 2011.
- [38] D. Turner, S. Savage, and A. Snoeren. On the empirical performance of self-calibrating wifi location systems. In *Local Computer Networks (LCN)*, 2011.
- [39] A. Varshavskya, E. d. Lara, J. Hightower, A. LaMarca, V. Otsason. GSM indoor localization. *Pervasive and Mobile Computing*, 2007.
- [40] H. Wang, S. Sen, A. Elgohary, M. Farid, M. Youssef, and R. R. Choudhury. Need to War-Drive: Unsupervised Indoor Localization. In *Mobisys*, 2012.
- [41] R. Want and et al. The Active Badge Location System. *ACM Transactions on Information Systems*, Jan. 1992.
- [42] C. Wu, Z. Yang, Y. Liu, and W. Xi. WILL: wireless indoor localization without site survey. In *INFOCOM*, 2012.
- [43] S-H Yang, E-M Jeong, D-R Kim, H-S Kim, Y-H Son and S-K Han. Indoor three-dimensional location estimation based on LED visible light communication. *Electronics Letters*, 49(1), Jan. 2013.
- [44] S-H. Yang, E-M. Jung, S-K. Han. Indoor location estimation based on LED visible light communication using multiple optical receivers. *IEEE Communications Letters*, 17(9), Sept. 2013.
- [45] Z. Yang, C. Wu, and Y. Liu. Locating in Fingerprint Space: Wireless Indoor Localization with Little Human Intervention. In *ACM Mobicom*, 2012.
- [46] M. Yoshino, S. Haruyama, and M. Nakagawa. High-accuracy Positioning System using Visible LED Lights and Image Sensor. In *IEEE Radio and Wireless Symposium*, 2008.
- [47] S. You, U. Neumann, and R. Azuma. Hybrid Inertial and Vision Tracking for Augmented Reality Registration. In *IEEE Virtual Reality* 1999.
- [48] M. Youssef and A. Agrawala. The Horus WLAN Location Determination System. In *MobiSys*, 2005.

APPENDIX A: PROOF OF THEOREM 1

Proof: Consider three linearly independent sensing planes, $A_i x + B_i y + C_i z = 0, 1 \leq i \leq 3$, that generate three nonzero RSS values s_1, s_2 and s_3 . Substituting these variables into Eq. 2 we can get a system of nonlinear equations:

$$\begin{cases} \frac{A'_1 x + B'_1 y + C'_1 z}{(x^2 + y^2 + z^2)^{3/2}} f_\omega \left(\arccos \frac{z}{\sqrt{x^2 + y^2 + z^2}} \right) = \frac{s'_1}{k} \end{cases} \quad (4)$$

$$\begin{cases} \frac{A'_2 x + B'_2 y + C'_2 z}{(x^2 + y^2 + z^2)^{3/2}} f_\omega \left(\arccos \frac{z}{\sqrt{x^2 + y^2 + z^2}} \right) = \frac{s'_2}{k} \end{cases} \quad (5)$$

$$\begin{cases} \frac{A'_3 x + B'_3 y + C'_3 z}{(x^2 + y^2 + z^2)^{3/2}} f_\omega \left(\arccos \frac{z}{\sqrt{x^2 + y^2 + z^2}} \right) = \frac{s'_3}{k} \end{cases} \quad (6)$$

where $A'_i = \frac{A_i}{\sqrt{A_i^2 + B_i^2 + C_i^2}}, B'_i = \frac{B_i}{\sqrt{A_i^2 + B_i^2 + C_i^2}}, C'_i = \frac{C_i}{\sqrt{A_i^2 + B_i^2 + C_i^2}}$, and $s'_i = s_i \in (0, s_m/k]$ or $s'_i = -s_i \in [-s_m/k, 0)$ depending on the symbol of $A'_i x + B'_i y + C'_i z$. Performing dividing among these equations gives

$$\begin{cases} (A'_1 - \frac{s_2}{s_1} A'_2)x + (B'_1 - \frac{s_2}{s_1} B'_2)y + (C'_1 - \frac{s_2}{s_1} C'_2)z = 0 \end{cases} \quad (7)$$

$$\begin{cases} (A'_1 - \frac{s_3}{s_1} A'_3)x + (B'_1 - \frac{s_3}{s_1} B'_3)y + (C'_1 - \frac{s_3}{s_1} C'_3)z = 0 \end{cases} \quad (8)$$

It can be shown that Eq. 7 and Eq. 8 are linearly independent, otherwise it can be verified that the vectors (A_i, B_i, C_i) are linearly dependent, which contradicts with the assumption. With this linear independence, we can represent x and y with z as $x = c_1 z$ and $y = c_2 z$, where c_1 and c_2 are functions of s_i, A_i, B_i and C_i . Substituting them into Eq. 4 and using the fact $z > 0$ can solve for z , which then gives x and y . Thus we obtain a unique solution of (x, y, z) . \square